

# Computational Simulation of Extravehicular Activity Dynamics during a Satellite Capture Attempt

Grant Schaffner\*, Dava J. Newman†

*Massachusetts Institute of Technology*

*Cambridge, Massachusetts 02139*

and

Stephen K. Robinson‡

*NASA Johnson Space Center, Houston, Texas 77058*

## Introduction

A more quantitative approach to the analysis of astronaut extravehicular activity (EVA) tasks is needed due to their increasing complexity, particularly in preparation for the on-orbit assembly of the International Space Station. Existing useful EVA computer programs either produce high resolution three-dimensional computer images based on anthropometric representations<sup>1,2</sup>, or empirically derived predictions of astronaut strength based on lean body mass and the position and velocity of the body joints<sup>3</sup>, but do not provide multi-body dynamic analysis of EVA tasks.

Our physics-based methodology helps fill the current gap in quantitative analysis of astronaut EVA by providing a multi-segment human model and solving the equations of motion in a high fidelity simulation of the system dynamics. The simulation work described here improves on the realism of previous efforts<sup>4</sup> by including astronaut three-dimensional motion, incorporating joint stops to account for the physiological limits of the range of motion, and making use of constraint forces to model object interaction.

To demonstrate the utility of this approach, the simulation is modeled on an actual EVA task, namely, the attempted capture of a spinning Intelsat VI satellite during STS-49 in May 1992. Repeated capture attempts by an EVA crewmember were unsuccessful because the capture bar could not be held in contact with the satellite long enough for the capture latches to fire and successfully retrieve the satellite.

---

\* Research Assistant, Department of Aeronautics and Astronautics, Room 33-119.

† Associate Professor of Aeronautics and Astronautics, Room 33-119. Senior Member AIAA.

‡ NASA Astronaut.

## Methods

The dynamic system model includes three elements: the satellite, capture bar, and astronaut (Fig. 1). A single rigid body represents the Intelsat VI satellite with 6 degrees-of-freedom (dof) initially rotating around the X (roll) axis at a rate of 1 rpm. The structural interface ring (where contact with the capture bar occurs) has a diameter of 2.35 m, and is located 1.34 m from the satellite's center of mass (in the X-direction). The capture bar is also represented by a single rigid body with six dof, and assistive v-guides are situated 2.35 m apart and the astronaut manipulation wheel has a diameter of 0.29 m. The center of mass of the capture bar is 0.81 m to the right of the center of the manipulation wheel and 0.31 m behind the front surface. The astronaut is modeled as a twelve-segment system: right and left lower leg, upper leg, upper arm, lower arm, and hand; plus the pelvis; and combined torso/head/backpack. Three dof ball joints define the ankle, hip, sacroiliac, shoulder, and wrist joints, while single dof hinge joints define the knees and elbows. The astronaut model has 31 dof, allowing full three-dimensional movement capability. The mass properties and joint parameters for the system are presented in Table 1.

The complete dynamic system (satellite, capture bar, and astronaut) has 43 dof. Since it is intractable to derive the equations of motion for such a complex multi-body system by hand, a commercial program (SD/FAST, Symbolic Dynamics Inc., Mountain View, California) was used to produce computer code representing the equations of motion. The simulation itself is run by computer code developed by the authors and is divided into two phases: an inverse-kinematics phase that uses the modeling and control schemes described below to compute the motion of the system, and an inverse-dynamics phase that uses these recorded motions to compute the astronaut's body joint torques.

During the inverse-kinematics phase, constraint forces are used to model the interaction between the capture bar and the satellite. As the capture bar comes into contact with the satellite, the amount of deviation,  $\delta_r$  and  $\delta_l$ , between the optimal contact points on the right and left sides, is found from

$$\begin{aligned}\delta_r &= v_{cr} - v_{sr} \\ \delta_l &= v_{cl} - v_{sl}\end{aligned}\tag{1}$$

where  $v_{cr}$  and  $v_{cl}$  are the global (inertial) reference frame transforms of vectors  $v'_{cr}$  and  $v'_{cl}$  (Fig. 1), which locate the contact points in the capture bar's body reference frame, and  $v_{sr}$  and  $v_{sl}$  are the

global transforms of  $v'_{sr}$  and  $v'_{sl}$ , which locate the contact points in the satellite's body reference frame.

The following discussion applies equally to right and left sides. During contact, constraint forces are modeled as springs and dampers acting in the normal and radial directions (defined by unit vectors  $n$  and  $r$  in Fig. 1)

$$\begin{aligned} F_n &= K_n \delta_n + B_n \dot{\delta}_n \\ F_r &= K_r \delta_r + B_r \dot{\delta}_r \end{aligned} \quad (2)$$

where  $F_n$  and  $F_r$  are the constraint forces,  $\delta_n$  and  $\delta_r$  the components of the deviation vector,  $K_n$  and  $K_r$  the stiffness coefficients, and  $B_n$  and  $B_r$  the damping coefficients, in the normal and radial directions, respectively. The values chosen for the stiffness and damping coefficients were obtained partly from material properties, and partly from trial and error. The final values used for  $K_n$  and  $K_r$  were 1000 N/m and 500 N/m, respectively, and 50 Ns/m was used for both  $B_n$  and  $B_r$ . The force in the tangential direction (unit vector  $t$  in Fig. 1) arises from friction between the rotating satellite ring and the capture bar

$$F_t = \mu F_n \quad (3)$$

where  $\mu$ , the coefficient of friction, was set at 0.25.

The forces exerted by the astronaut on the capture bar in the normal direction are modulated by proportional-plus-derivative (PPD) control

$$F_{Hn} = C_p(R - e) + C_d v \quad (4)$$

where  $R$  is the astronaut's maximum reach (0.67 m from shoulder to mid-palm),  $e$  is the actual arm extension,  $v$  is the velocity of extension, and  $C_p$  and  $C_d$  are the proportional and derivative constants, set at 44 N/m and 50 Ns/m, respectively. The forces exerted by the astronaut in the tangential direction are calculated to provide a counter-rotary moment that balances the frictional forces on the capture bar. For the right side, this force is

$$F_{HtR} = \frac{1}{2r_w} [(r_s - r_w)F_{tL} + (r_s + r_w)F_{tR}] \quad (5)$$

where  $r_s$  and  $r_w$  are the radii of the satellite interface ring and the capture bar manipulation wheel, respectively, and  $F_{tL}$  and  $F_{tR}$  are the left and right sided tangential forces, respectively.

It is assumed that the astronaut's feet are fixed in the inertial reference frame (i.e., clamped to the Space Shuttle foot restraint) and his hands are attached to each side of the capture bar's

manipulation wheel. Only the forces exerted by the astronaut's hands are prescribed (rather than prescribing joint angles in a forward kinematics approach) since this mimics the actual task as described during EVA training.

All of the body joints are subject to passive proportional-plus-derivative control during the inverse kinematics phase, to model human muscular actuation. In the nominal range (Eq. 6), the torque,  $\tau_j$ , biases the joint angle,  $q_j$ , toward a predetermined value,  $q_b$ . The subscript,  $j$ , is an index to indicate that there is a separate equation for each joint and each degree of freedom. When the joint exceeds the limits of its motion,  $q_l$ , it encounters joint stops modeled as stiff springs (Eq. 7), with  $k_l$  set at 17.45 Nm/deg for all joint axes. The values for the nominal range spring constants,  $k_j$ , and damping,  $b_j$ , and the limit springs,  $k_l$ , are given in Table 1.

$$\tau_j = -k_j(q_j - q_b) - b_j\dot{q}_j \quad (6)$$

$$\tau_j = -k_l(q_l - q_j) \quad (7)$$

In the lower body joint (sacroiliac to ankle) constants are higher to maintain posture, while the arm joint constants are lower because the arms carry out most of the required motion. Since there are many redundant dof, body joint angles are found using a linearized least squares root solver.

## Results

Figure 2 shows the motion of the capture bar. An initial negative yaw is quickly reversed as the left v-guide makes contact with the satellite at 0.8 s, followed by contact with the right v-guide at about 1.3 s. The X-translation shows initial forward acceleration, during the first 1.5 s, followed by some rebound and settling against the satellite interface ring, and then a sustained push to the limit of the astronaut's reach envelope. The initial configuration of the astronaut's arms was 0.51 m of extension, therefore, the remaining 0.16 m of his reach envelope are quickly depleted. Contact between the capture bar and satellite begins at 0.7 s and lasts until 6.3 s.

Under pressure from the capture bar, the satellite accelerates away from the astronaut at 0.12 m/s<sup>2</sup> and acquires a final X-velocity of 0.047 m/s. In addition, the satellite spin (roll) velocity is reduced from 6.02 to 5.55 deg/s and yaw and pitch rates of -0.023 deg/s and 0.011 deg/s are imparted.

Figure 3 shows astronaut body joint positions. The arms extend close to the limit of the astronaut's reach, where contact is lost with the satellite, and the shoulder, elbow, and wrist Z-axis

rotations stabilize around 80 deg, 10 deg, and -10 deg, respectively. The remaining degrees-of-freedom are not shown in Fig. 3 because they deviate less than 5 deg from the starting values.

Joint torques calculated during the inverse dynamics phase were found to be well within the astronaut's strength limits (100 to 200 Nm for most joint dof). In general, the greatest torques are experienced in the leg joints: -10.27 Nm in the left ankle, and -10.28 Nm in both the left knee and left hip. The largest torque experienced in the upper body was 8.98 Nm in the left shoulder.

### **Discussion**

The primary goal of this research effort was to demonstrate that a relatively complex EVA task could be simulated using computational multi-body dynamics. The objective was not to showcase the full range of capabilities of computational simulation, but rather to establish a testbed that could be used for further exploration of simulation techniques. While the dynamic system itself is of a relatively high fidelity, there are remaining limitations. Most notable among these is the use of simple control laws to model astronaut hand forces and body torques. There exists an opportunity for additional work on simulations that employ more advanced control, including theory to account for the intelligence of the astronaut. Other limitations that should be addressed in future studies include: a more scientific approach to the selection of control parameters and other constants; the influence of the EVA spacesuit on joint mobility; and compliance in the anchoring of the astronaut's feet (such as that expected from a portable foot restraint attached to the Orbiter's Remote Manipulator System). In spite of these limitations, some important conclusions can be derived from this work.

Figure 2 shows that the asymmetrical location of the capture bar center of mass causes an initial yaw motion that brings the left side of the capture bar into contact with the satellite before the right side. As a result, roll and pitch disturbances are introduced which, together with the rebounds caused by the relatively non-compliant interface between the v-guides and the satellite interface ring, make it difficult for the astronaut to maintain the proper alignment between the capture bar and the satellite. In addition, the contact duration of 5 to 6 seconds was not sufficient to allow the satellite to rotate to the position where the capture bar latches would be triggered by structural elements on the satellite, an observation confirmed by video footage of STS-49. Furthermore, the slowing of the satellite spin due to friction with the capture bar, and the yaw and pitch rates caused

by the unequal forces at the left and right contact points (also a consequence of the capture bar center of mass asymmetry), could complicate further EVA capture attempts.

The fact that the satellite quickly translates out of reach when force is applied, combined with the observation of low body joint torque values indicates that a very light touch is required for this type of EVA task. This may be difficult since, according to EVA crewmembers, the spacesuit restricts tactility and proprioception, making it difficult to exert precision forces below a certain threshold (estimated to be as much as 40N in the spacesuit).

A number of recommendations are suggested by the results of this simulation. For this type of task, astronauts should use very small, precise forces, even when dealing with objects of large mass. To compensate for the limited tactility allowed by a spacesuit, a mechanism such as the capture bar should be designed with additional compliance and minimal friction at the contact interface. Wherever possible, the center of mass of the manipulated object should be aligned with the center of the astronaut's task coordinates (i.e., the center of the manipulation wheel), even if this means adding more mass. Finally, physical and computational simulators should be used in conjunction during EVA training so that each may help compensate for the limitations of the other.

### **Acknowledgments**

The authors wish to thank David Rahn and for his computer animation work; our collaborators Norman Badler and Dimitris Metaxas from the University of Pennsylvania, Robert Callaway and Bruce Webbon from NASA Ames Research Center and Mike Rouen, Joe Kosmo, Robert Trevino, Jim Maida, and Abilash Pandya from NASA Johnson Space Center for their encouragement and support; and Mike Sherman and Dan Rosenthal of Symbolic Dynamics for technical assistance. This research effort is supported under NASA Grants NAGW-4336, NAG5-4928, NAG5-3990.

### **References**

<sup>1</sup>Price, L. R., Fruhwirth, M. A., and Knutson, J. G., "Computer Aided Design and Graphics Techniques for EVA Analysis," *Proceedings of the Twenty-Fourth International Conference on Environmental Systems and Fifth European Symposium on Space Environmental Control Systems*. (Friedrichshafen, Germany), Technical Paper No. 941558. Society of Automotive Engineers, Warrendale, PA, June 1994, pp. 1-13.

<sup>2</sup>Anon., "The McDonnell Douglas Human Modeling System MDHMS," Version 2.2., McDonnell Douglas Report. MDC-93K0283, McDonnell Douglas Aerospace-West, McDonnell Douglas Corporation, MDC-93K0293, Long Beach, CA, Sept. 1993, pp. 1-35.

<sup>3</sup>Pandya, A. K., Hasson, S. M., Aldridge, A. M., Maida, J. C., and Woolford, B. J., "Correlation and Prediction of Dynamic Human Isolated Joint Strength From Lean Body Mass," NASA TD-3207, June 1992.

<sup>4</sup>Newman, D. J., and Schaffner, G., "Computational Dynamic Analysis of Extravehicular Activity (EVA): Large Mass Handling," *Journal of Spacecraft and Rockets*, Vol. 35, No. 2, 1998, pp. 225-227.

**Table 1 Mass properties for all segments and objects in the dynamic system**

Segment/ Object	Mass, kg	Moments of Inertia, kgm <sup>2</sup> (body-fixed coordinates)			Joint	Initial Angle (Right/Left), deg		
		I <sub>xx</sub>	I <sub>yy</sub>	I <sub>zz</sub>		Roll	Yaw	Pitch
Intelsat	4065.00	6781.000	6114.000	6140.000	6dof			
Capture Bar	73.21	71.763	87.579	15.869	6dof			
Hand	.53	.001	.001	.001	Wrist	0/0	0/0	-55/-55
Forearm	1.45	.009	.001	.010	Elbow			90/90
Upper arm	2.05	.014	.003	.015	Shoulder	-90/90	0/0	0/0
Head	5.50	.021	.015	.024				
Trunk	28.61	.531	.332	.392	Sacroiliac	0	0	0
PLSS	66.46	5.497	2.043	3.813				
Pelvis	12.30	.112	.130	.104	Hip	0/0	0/0	-45/-45
Upper leg	10.34	.170	.046	.178	Knee			45/45
Lower leg	4.04	.062	.007	.063	Ankle	0/0	0/0	0/0

Source: NASA

**Table 1 Mass, inertia, angle, stiffness, and damping properties for all objects in the dynamic system**

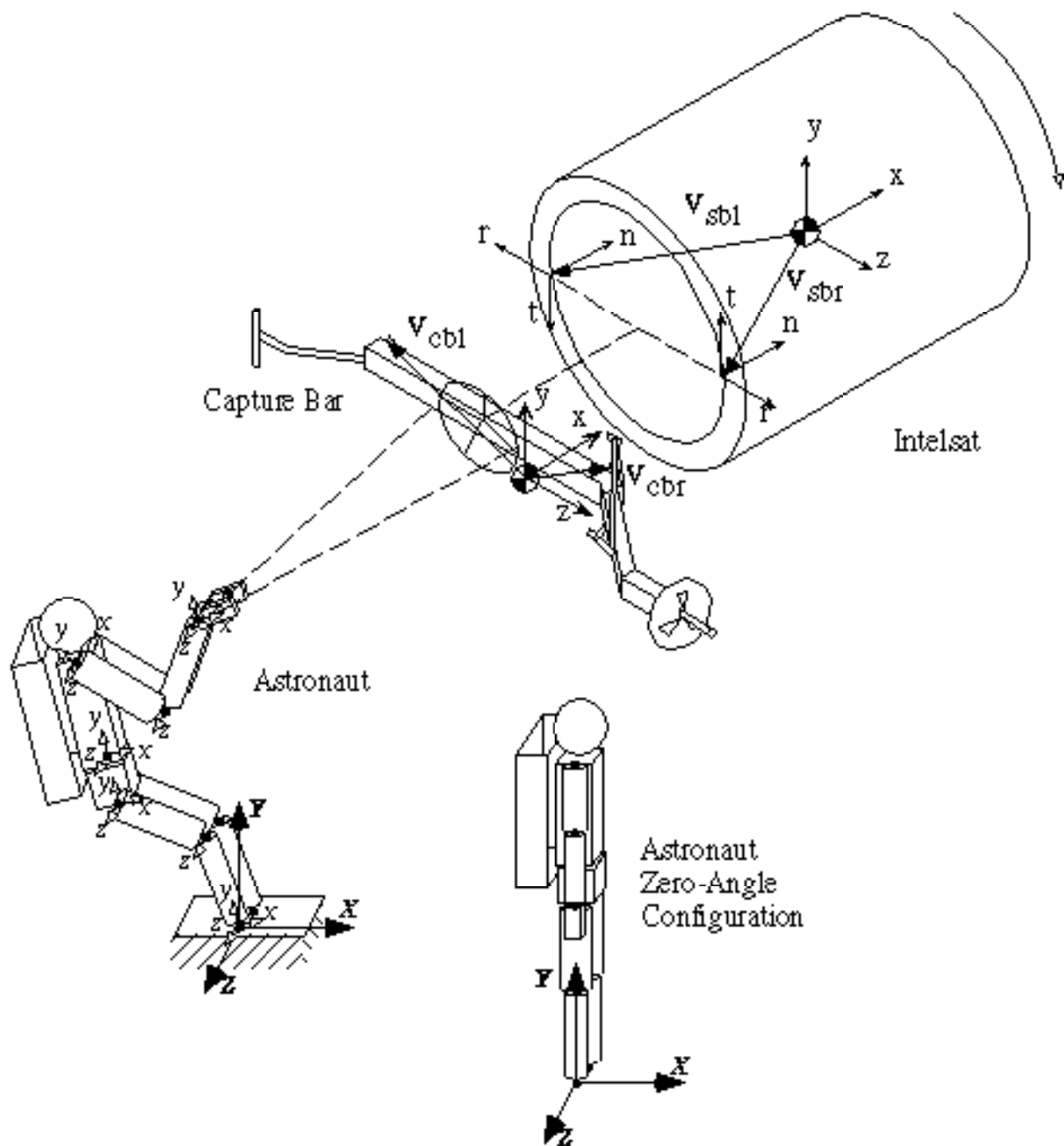
Stiffness, $k$	Damping, $b$
Nm/deg	Nms/deg
–	–
–	–
0.70	0.35
0.70	0.35
0.70	0.35
–	–
3.49	0.35
–	–
3.49	0.35
3.49	0.35
3.49	0.35

Figure 1. Dynamic system: multi-body astronaut model, Intelsat VI satellite, and capture bar.

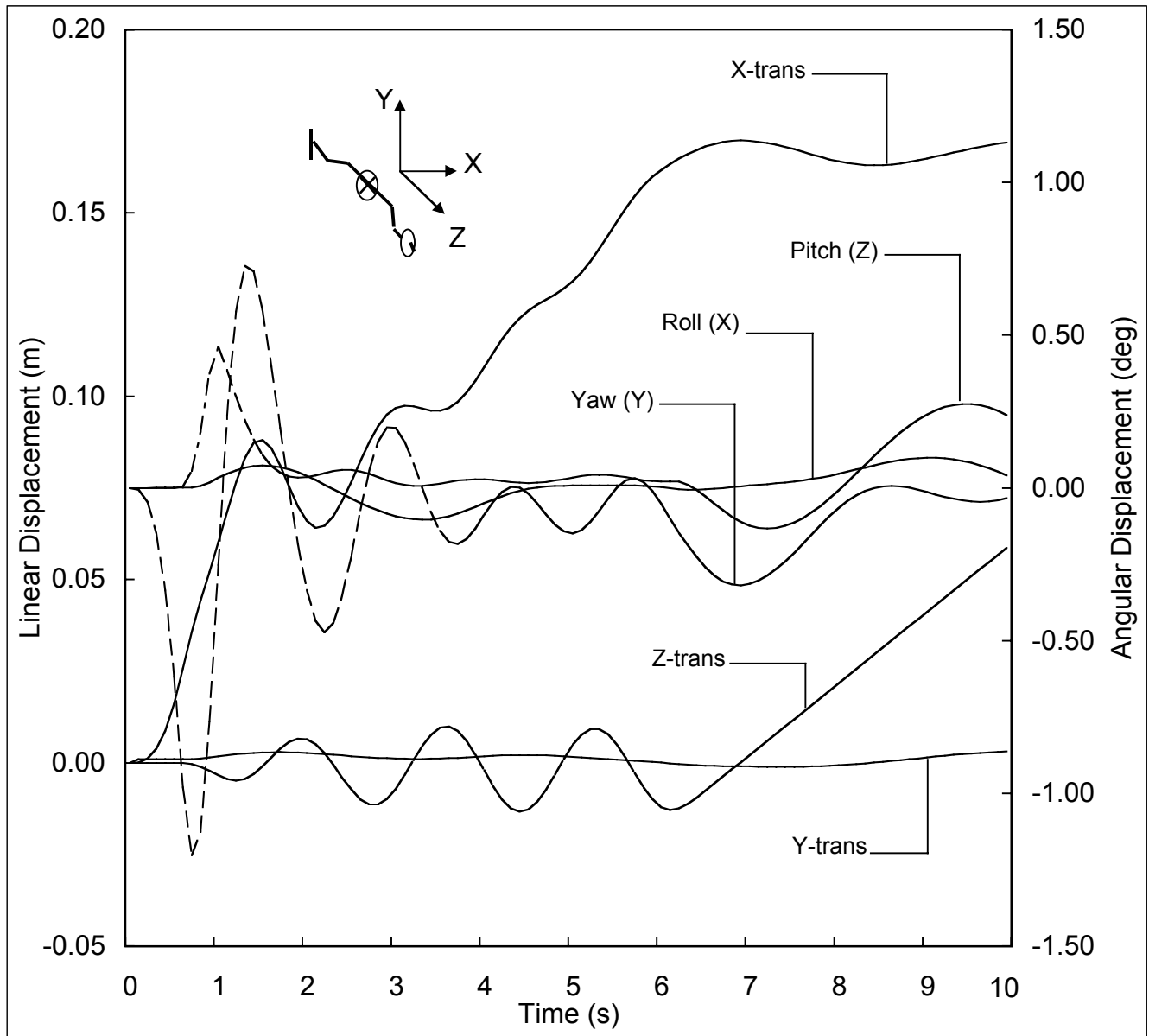
Figure 2. Capture bar position vs. time plot.

Figure 3. Astronaut body joint position vs. time plot.

Schaffner, Newman, and Robinson, Figure 1



Schaffner, Newman, and Robinson, Figure 2



Schaffner, Newman, and Robinson, Figure 3

